JOURNAL OF PROPULSION AND POWER
Vol. 12, No. 2, March–April 1996

Flow Visualization and the Three-Dimensional Flow in an Axial-Flow Pump

W. C. Zierke* and W. A. Straka†
Pennsylvania State University, State College, Pennsylvania 16804

Surface flow visualization on an axial-flow pump results in patterns of the skin-friction lines on various surfaces and these patterns provide important insight into the topology of the three-dimensional flowfield. In particular, critical points and lines within the patterns give characteristics of three-dimensional separation and the formation of vortical structures. Here, oil-paint tests show the topology for the formation of horseshoe vortices, the structure of three-dimensional corner separation, the initial development of a rotor tip leakage vortex, and the development of other important secondary flows. Surface flow visualization can also provide information concerning boundary-layer transition. In summary, the surface flow visualization experiment presented in this article allows one to give a fairly detailed description of the complex flow within an axial-flow pump.

Introduction

THE separation of three-dimensional, turbulent boundary layers leads to the formation of vortical structures within the flowfield. Within a turbomachine, these secondary flows result in total-pressure losses and deviations in flow turning. Before one attempts to quantify these secondary flows by acquiring measurements in the flowfield itself, a careful interpretation of patterns obtained from surface flow visualization can give a reasonable description of the secondary flows generated by separation.

For the incompressible flow of water through an axial-flow pump, oil-paint methods give reliable surface flow visualization patterns. If one covers either entire surfaces or spots on surfaces with a thin coat of oil-paint, the shear stress within the flow will carry the oil-paint with it and, in time, will establish a persistent pattern. In a similar oil-streak flow visualization technique, Squire[1] showed that the direction of the resulting streaks passing through a point on a surface is very close to the direction of the skin-friction line passing through the same point. Tobak and Peake[2,3] also concluded that surface flow visualization patterns should be interpreted as being representative of skin-friction lines. Skin-friction lines are very similar to limiting streamlines, which result in the limit as the height between external streamlines and the surface approaches zero. As long as these limiting streamlines remain parallel to the surface, they remain indistinguishable from skin-friction lines. However, in the vicinity of lines of separation, limiting streamlines can rise rapidly and leave the surface. Since lines of separation are themselves skin-friction lines, surface flow visualization patterns may not give an indication of limiting streamlines near regions of separation.

In some regions of separation, the streamwise pressure gradient strongly affects the oil-paint flow by decelerating the flow, thickening the oil-paint film, and causing the oil-paint to accumulate. Tobak and Peake[2,3] call this a local separation line, of which a two-dimensional separation line is a good example. If local reattachment occurs, the oil-paint accumulation will stop as the shear stress increases. One must take care when interpreting an oil-paint accumulation region as laminar separation and turbulent reattachment, since the oil-paint pattern might be indicating a region of natural or bypass transition instead. The wall shear stress at the beginning of transition can be quite small and cause the oil-paint film to thicken. Through the transition region, the wall shear stress increases to the point where the turbulent shear stress removes the oil-paint film much quicker. Therefore, the oil-paint accumulation can indicate natural or bypass transition, although a stronger dependency on oil-paint thickness and run time, combined with the fact that the wall shear stress always remains finite, make transition (especially the end of transition) more difficult to resolve than separation using the oil-paint method.

To apply this type of surface flow visualization technique to rotating blades, one must be assured that the centrifugal force does not affect the oil-paint in a different manner than it affects the actual fluid. Arakawa and Tagori[4] investigated this concern with some fundamental experiments using a rotating disk and a more practical experiment using an axial-flow pump. Using water as the working fluid, they performed surface flow visualization with oil films of different specific gravities and compared the results with three-dimensional boundary-layer calculations. As might be expected, the reduction of the specific gravity of the oil film towards that of water gave measured skin-friction lines closer to the calculated skin-friction lines. The reduction in rotor speed Ω and the increase in Reynolds number $r^2\Omega/\nu$ also gave better comparisons. For this investigation, we combined gear oil with paint, which itself is a combination of linseed oil and pigment. Both the gear oil and linseed oil have a specific gravity near 0.94 (compared to 1.0 for water). The addition of pigment will add color and should increase both the specific gravity and kinematic viscosity. The increased specific gravity should give a specific gravity of the oil-paint close to that of water, making the added effect of centrifugal force almost negligible. Therefore, this surface flow visualization technique becomes applicable to blades rotating through water, and it is not applicable for blades rotating through air. The very high kinematic viscosity of the oil-paint increases the time to establish a persistent pattern, but allows photographs to be taken later without the effect of gravity damaging the pattern.

Interpretation of surface flow visualization patterns can be quite subjective, with a strong dependence on the quality of the patterns. Also, surface flow visualization methods have essentially zero-time response and give no information on the flow unsteadiness. However, Tobak and Peake[2,3] and Délery[5]

Received Jan. 5, 1995; revision received July 28, 1995; accepted for publication Aug. 8, 1995.

*Research Associate, Applied Research Laboratory, Fluid Dynamics and Turbomachinery Department, P.O. Box 30.

†Research Assistant, Applied Research Laboratory, Fluid Dynamics and Turbomachinery Department, P.O. Box 30. Member AIAA.

have shown that the application of topological rules to these patterns creates a rational way of understanding time-average, two- and three-dimensional, viscous flows. Their views are based on the work of Lighthill[6] and Legendre[7] that view surface flow visualization patterns as skin-friction lines rather than limiting streamlines. Skin-friction lines (and the associated orthogonal surface vortex lines) behave as continuous vector fields that are characterized by critical or singular points, points where the shear stress is zero.

Only two types of singular points exist: 1) nodal points and 2) saddle points. A nodal point is common to an infinite number of skin-friction lines that either leave the node, as in a nodal point of separation, or enter a node, as in a nodal point of attachment. If the node has no common tangent line and the skin-friction lines either leave or enter the node in a spiral motion, the node is called a spiral node or focus. Skin-friction lines originate typically at nodal points of attachment and can disappear into nodal points of separation. Since skin-friction lines springing from adjacent nodal points of attachment will tend to run into each other, there must exist between them a saddle point, emanating from which a single skin-friction line will act as a barrier between the skin-friction lines from the adjacent nodal points and prevent crossing. Only two skin-friction lines, or critical lines (separators), pass through a saddle point. If the adjacent skin-friction lines tend to converge asymptotically onto one of these critical lines, we refer to it as a line of separation (a line near which adjacent limiting streamlines will tend to leave the surface). In regions of larger adverse pressure gradients, the adjacent skin-friction lines will converge faster and the adjacent limiting streamlines will take-off more rapidly. Skin-friction lines diverge asymptotically from the other critical line, which is called a line of attachment, and this pattern will be accentuated in regions of larger favorable pressure gradients. The resulting patterns can provide a three-dimensional skeleton structure of the viscous flow. On an isolated three-dimensional surface, Lighthill[6] determined that the number of nodal points must exceed the number of saddle points by two. Actually, Perry and Fairlie[8] and Hunt et al.[9] showed that singular points also exist within the external flowfield and additional topological rules apply when considering these external singular points in addition to the surface singular points. Some internal flows also have different topological rules.

Finally, patterns obtained from the surface flow visualization provide excellent results to compare with numerical predictions. Typically, one uses predicted particle path lines either one or two grid points off the surface to approximate limiting streamlines. More interesting comparisons with experimental patterns would use predicted skin-friction lines, as well as these predicted path lines. These comparisons would help answer the questions of how well the predicted path lines and skin-friction lines compare in the vicinity of separation. Also, better comparisons with the experimental patterns should result in better numerical predictions of the three-dimensional structures within the flowfield. For this particular experiment, comparisons with the patterns from the surface flow visualization should be followed by comparisons with some detailed flow measurements reported by Zierke et al.[10,11]

Axial-Flow Pump Experiment

This axial-flow pump experiment was performed in the Garfield Thomas Water Tunnel at the Applied Research Laboratory at the Pennsylvania State University. The tunnel has a 1.22-m-diam, 4.27-m-long test section that supports water velocities up to 18.29 m/s and static pressures ranging from 20 to 414 kPa. For this experiment, we used the high Reynolds number pump (HIREP) facility, which consists of a 1.07-m-diam pump stage driven by a 1.22-m-diam downstream turbine. The hub has a constant diameter of 0.53 m. The two units rotate together on a common shaft in the test section of the water tunnel, such that the main drive impeller of the tunnel overcomes the energy losses within HIREP. The pump includes a row of 13 inlet guide vanes, a row of seven rotating blades, and three downstream support struts. Farrell et al.[12] give a more detailed explanation of the HIREP facility.

Zierke et al.[10] give a detailed explanation of this experiment. However, some geometric characteristics should be noted here. Each inlet guide vane (IGV) and rotor blade trailing-edge geometry is essentially an asymmetric chisel, with the bevel of the chisel lying on the suction side of the blade and the point of the chisel being somewhat rounded off. All of the inlet guide vanes and rotor blades include fillets where the blades meet the endwalls. Also, each rotor tip section includes a rounded pressure side corner, with a radius of curvature of approximately 25% of the local blade thickness. Gearhart[13] found that this rounded corner prevented local separation of the flow through the tip clearance and, thus, improved the gap cavitation performance. The rotor blades are designed with a significant negative blade circumferential lean (such that the suction surface points toward the hub surface), as shown in Fig. 1. Table 1 summarizes the geometry and flow parameters used during this HIREP experiment.

Surface flow visualization tests were run after initial tests indicated the optimum oil-paint mixture and thickness as well as the tunnel run time. After each test we photographed the

Table 1 Geometry and flow parameters for HIREP

Parameter	IGVs	Rotor blades
Blade number	13	7
Chord, c	0.18 m	0.29 m, hub 0.27 m, tip
Maximum blade thickness, t_{max}/c	11.6%	17.8%, hub 10.0%, tip
Solidity	1.36, hub 0.68, tip	1.19, hub 0.56, tip
Hub radius	0.27 m	0.27 m
Tip radius, nominal	0.53 m	0.53 m
Blade chord Reynolds number, $Re_{c\,tip} = W_1 c_{tip}/\nu$	2.3×10^6	5.5×10^6
Rotor tip clearance, h/c_{tip}	——	1.24%
Diffusion factor	——	0.28, hub 0.12, tip
Reference velocity, V_{ref}	10.7 m/s	
Rotor rotational speed	260 rpm	
Rotor tip velocity, U_{tip}	14.5 m/s	
Flow coefficient, $\phi = V_{ref}/U_{tip}$	0.74	
Axial component of freestream turbulence intensity level	0.107 ± 0.006%	

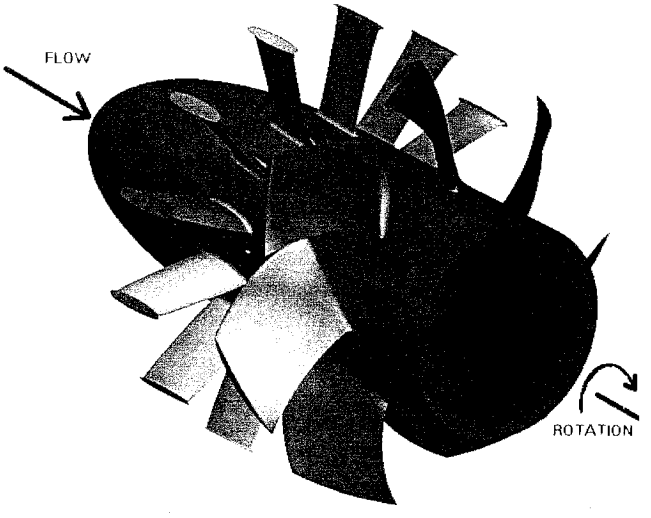

Fig. 1 Computer-generated isometric view of the HIREP blades.

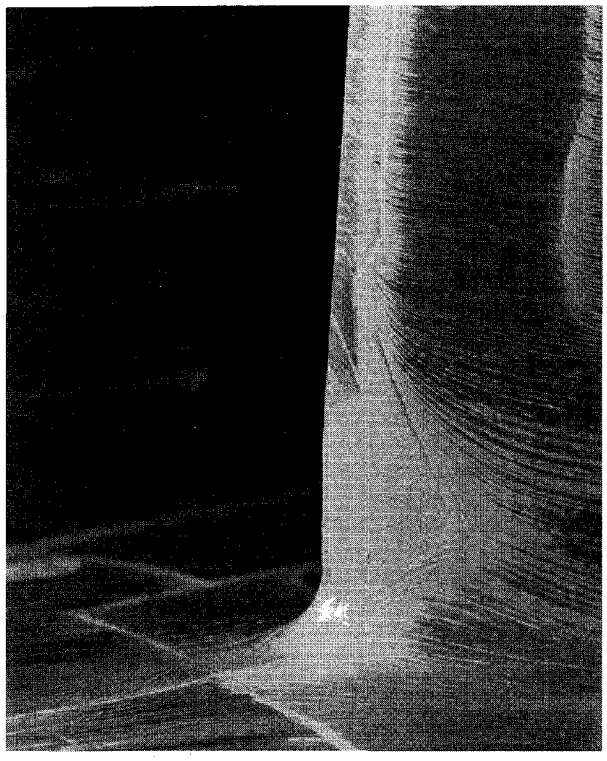

Fig. 2 Photograph of the surface flow visualization showing the IGV suction surface trailing-edge corner separation near the hub (fluid flows from right to left).

patterns from many different angles and physically measured the distances from significant oil-paint regions (such as singular points) to known geometric references. A representative photograph of the oil-paint near the IGV hub trailing edge is shown in Fig. 2. Oil-paint visualization was completed on the suction and pressure surfaces of both inlet guide vanes and rotor blades, on the hub surfaces of both the inlet guide vanes and rotor blades, on the inside surface of the IGV indexing ring (which fits flush with the outer tunnel liner), and on the tip section of the rotor blades. Other measurements by Zierke et al.[10] showed that the inlet guide vanes have a chord Reynolds number of 2.3×10^6. Meanwhile, the chord Reynolds numbers for the rotor blades range from 3.6×10^6 at 90% span up to 3.9×10^6 at 10% span. More appropriately, using relative velocities, the chord Reynolds numbers range from 5.5×10^6 at 90% span down to 4.1×10^6 at 10% span.

Results on the Inlet Guide Vanes

Before attempting to interpret the IGV surface flow visualization patterns, we first analyzed hundreds of photographs together with physical length measurements taken immediately after each test. The resulting patterns have been drawn on various projected surfaces. Figure 3 shows the reconstruction of the oil-paint pattern on the hub surface of the inlet guide vanes. The dark gray surface with the bold black border represents a footprint of the designed blade section at the hub, while the light gray region surrounding this blade section represents the extension of the fillet onto the hub surface. The inlet and exit flow vectors in Fig. 3 are the design flow vectors at the hub as determined from a streamline curvature solution.

The first region of interest in Fig. 3 is the region on the hub surface near the blade leading edge. Just upstream of the point where the leading-edge fillet merges into the hub surface, one can identify a saddle point. Between the saddle point and the blade leading edge, the skin-friction lines move upstream and, despite the fact that the oil-paint photographs were not as distinct in this region, one must surmise that a nodal point of attachment exists somewhere on the blade leading edge. The critical skin-friction line that passes through the saddle point and forms a C-pattern around the blade is a line of separation. In general, as the fluid approaches the blade, the flow will slow down and stagnate somewhere near the blade leading edge, creating an adverse pressure gradient. Within the endwall boundary layer on the hub, this adverse pressure gradient causes the boundary layer to separate, with the point of zero shear stress occurring at the saddle point. As the two legs of the separation line bend around the blade, the vorticity in the separated boundary layer rolls-up to form what is commonly called a horseshoe vortex or necklace vortex. Alternatively, one could represent the hub boundary layer as a vortex line in the circumferential direction. This vortex line convects downstream around the blade leading edge, resulting in segments of this vortex line on each side of the blade with vorticity in the streamwise direction, or a horseshoe vortex.

Past investigations have shown that the formation of vortices other than the primary horseshoe vortex can occur in the leading-edge region. However, we could not identify the additional singular points required for the formation of these other vortices. Also, other investigators have identified another C-shaped skin-friction line between the leading edge and the separation line passing through the saddle point. This additional skin-friction line is usually easier to identify than the separation line because of an accumulation of the substance used in the surface flow visualization test. For flow around a circular cylinder, Baker[14] and Eckerle and Langston[15] claim that this line is a secondary line of separation (or a local separation line) associated with the roll-up of the horseshoe vortex. For flow in a wing–body junction, Devenport and Simpson[16] claim that this line is a line of low streamwise shear (not a line of separation or reattachment) and that this line merges into the separation line somewhere downstream. In our case, we could not identify this second skin-friction line from an accumulation of oil-paint. Again, remember that the oil-paint photographs were not as distinct in this region. Perhaps this line coincides very closely with the separation line passing through the saddle point. Another point of interest is the effect of the fillet on the formation of the horseshoe vortex. Devenport et al.[17] performed a study of this effect in the flow past a wing–body junction. Essentially, the fillet simply increased the radius of the leading edge and displaced the horseshoe vortex a little further from the wing. They also measured a small increase in the size and strength of the horseshoe vortex when a fillet was present.

Most previous investigations of horseshoe vortices through surface flow visualization and other experimental techniques have focused either on nonlifting bodies, such as cylinders or struts, or on turbine blades with a large amount of flow turning.

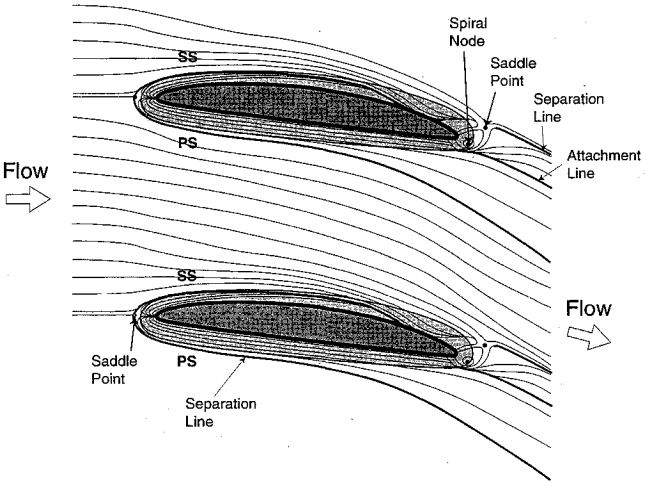

Fig. 3 Schematic of surface flow visualization on the IGV hub surface. SS = suction surface and PS = pressure surface.

However, a few investigators have shown surface flow visualization patterns of the horseshoe vortex around compressor blades, lifting bodies with only a small amount of flow turning. Dong et al.[18] showed a pattern on a rotor hub surface, while Schulz and Gallus[19] showed a pattern on a stator hub surface. Both of these patterns were very similar to our surface flow visualization pattern in Fig. 3. In all of these cases, the pressure side leg of the horseshoe vortex separation line moved downstream into the midpassage region. For the case of a large turning turbine blade, Sieverding[20] shows that the pressure side leg of the separation line moves far enough from the blade that it actually interacts with the suction surface of the adjacent blade, creating a corner vortex. Also in agreement with the compressor blade patterns, Fig. 3 shows that the suction side leg of the separation line moves up onto the suction surface. This movement is the result of the flow overturning in the hub endwall region.

As fluid passes through any turbomachine blade passage, the turning flow creates a circumferential pressure gradient. Within the endwall boundary layer, the momentum of the flow is reduced and the flow cannot follow the turning flow path as imposed by the blade design. The circumferential pressure gradient causes the flow to overturn, and this, subsequently, causes the suction side leg of the horseshoe vortex separation line to move up onto the suction surface. Figure 3 shows the overturning of the flow exiting the inlet guide vanes by comparing the oil-paint pattern with the design flow angle. This overturning flow also initiates the vortical motion that results in the classical secondary flow called a passage vortex. Again, representing the endwall boundary layer as a vortex line, the turning of the vortex line through the blade passage yields a component of vorticity in the streamwise direction, vorticity that makes up the passage vortex. The vortical motion that initiates the passage vortex rotates the flow in the same sense as the pressure side leg of the horseshoe vortex. In their turbine blade cascade, Sieverding and Van den Bosch[21] used colored smoke visualization to show that the pressure side leg of the horseshoe vortex simply merges into the passage vortex. The suction side leg of the horseshoe vortex rotates with the opposite sense and wraps around the passage vortex.

Figure 4 shows the reconstruction of the oil-paint pattern on the suction surface of an inlet guide vane. For the most part, the flow on the suction surface appears to be two dimensional. The vertical dotted lines enclose a region where the oil-paint accumulated, which would indicate either transition or a separation bubble. Since the IGV static-pressure distribution of Zierke et al.[10] shows no sign of an adverse streamwise pressure gradient in this region, one would expect the oil-paint accumulation to indicate natural transition. The oil-paint pattern indicates that transition should begin near 18% chord and end near 41% chord. To corroborate this observation, Zierke et al.[10] calculated that transition should begin and end at 15 and 30% chord, respectively. Recall that the oil-paint method should give a better indication for the beginning of transition than for the end of transition. In fact, the downstream end of this oil-paint accumulation did vary with different run times used from test-to-test.

Proceeding downstream near the hub, one notices flow moving from the hub endwall up onto the suction surface as a result of the flow overturning. A saddle point occurs near 88% chord and 6% span. The separation line passing through this saddle point moves downstream, with one leg moving up the span and the other leg moving back toward the hub. This latter leg of the separation line probably moves back up the suction surface and into the spiral node located near 97% chord and 3% span. Another spiral node, near 95% chord and 8% span, also exists within this three-dimensional corner separation. The flow entering this second spiral node seems to have originated in the pressure surface boundary layer, turned around the trailing edge, and moved upstream on the suction surface. Schulz and Gallus[19] also found skin-friction lines moving around the

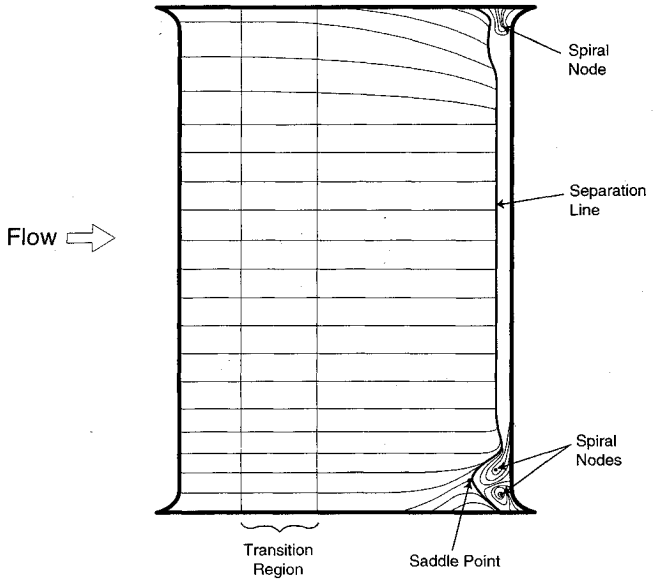

Fig. 4 Schematic of surface flow visualization on the IGV suction surface.

trailing edge and upstream along the suction surface. However, their corner separation, as well as the ones found by Dong et al.[18] and Joslyn and Dring,[22] were much larger with more backflow and more radial outflow. These compressor studies were made with higher-loaded blades that resulted in more overturning of the flow on the hub endwall and, hence, a larger corner separation region. Also, the inlet guide vanes used in this study are an accelerating blade row that would tend to minimize separation.

The separation line passing through the saddle point on the suction surface of Fig. 4 forms the three-dimensional corner separation. This is also shown in Fig. 2. Beginning at the saddle point and moving along the legs of the separation line, the limiting streamlines will leave the surface and form a dividing surface of separation. A concentrated vortex filament will extend into the external flowfield from each of the spiral nodes. Then, the dividing surface of separation will roll-up around each of these vortex filaments and convect downstream. Therefore, the vortical cores about which these dividing surfaces coil begin at spiral nodes. In this case, the three-dimensional corner separation also contains a secondary separation. Near this corner on the hub surface, Fig. 3 shows the existence of another saddle point just downstream of the trailing edge. One leg of the separation line proceeds downstream and, beginning at the saddle point, the limiting streamlines leave the hub surface along this line to form a dividing surface of secondary separation. Again, the vortical core about which this dividing surface coils begins at the spiral node located in the trailing-edge region of Fig. 3. Also, note that the skin-friction lines converging asymptotically onto this secondary separation line seem to be emanating from a nearby attachment line.

Further, radially outward on the IGV suction surface of Fig. 4 at about 19% span, one finds that the trailing-edge separation pattern changes. Photographs of this region showed a significant accumulation of oil-paint and, following Tobak and Peake,[2,3] we refer to this line as a line of local separation, which in this case represents two-dimensional separation. This two-dimensional separation occurs over the last 5% chord, a separation forced by the chisel trailing edge. Boundary-layer calculations also showed the likelihood of this trailing-edge separation. Near the IGV tip, at about 96% span and 97% chord, one finds another spiral node of separation. The separation line entering this spiral node passes through a saddle point near the IGV trailing edge on the casing endwall, as seen in Fig. 5. Figure 5 shows that the other leg of the separation

line passing through this trailing-edge saddle point proceeds downstream and, beginning at the saddle point, the limiting streamlines leave the casing surface along this line to form a dividing surface of separation. The vortical core about which this dividing surface coils begins at the spiral node located in the trailing-edge region of Fig. 4. As was the case on the hub endwall, the skin-friction lines converging asymptotically onto this separation line on the casing endwall in Fig. 5 seem to be emanating from a nearby attachment line.

The reconstruction of the oil-paint pattern on the casing endwall of Fig. 5 shows a topology for the formation of the horseshoe vortex that is nearly identical to the topology on the hub endwall. Again, a saddle point exists just upstream of the leading edge and a nodal point of attachment probably exists on the leading edge itself. The pressure side leg of the separation line passing through this saddle point moves downstream into the midpassage region, while the suction side leg moves downstream and then onto the suction surface because of the overturning of the flow in the casing boundary layer. Notice the radial downward flow near the tip region of the IGV suction surface in Fig. 4. The blade section at the IGV tip is designed for less fluid turning than the root blade section. Therefore, the skin-friction lines on the casing endwall show less overturning than the skin-friction lines on the hub endwall and the resulting passage vorticity should not be as large. While the suction side leg of the separation line never migrated beyond the outer edge of the blade fillet on the hub endwall, the suction side leg moved well beyond the fillet on the casing endwall, before moving back onto the suction surface. A larger endwall boundary layer and a smaller amount of overturning within this boundary layer contribute to this difference in topology.

Zierke et al.[10] showed that the incoming endwall boundary layer on the casing was much larger than the boundary layer on the hub endwall. And yet, the skin-friction lines on both endwalls show that the topology for the formation of the horseshoe vortex is nearly identical. Other investigators have also shown that, qualitatively, the structure of this three-dimensional separation does not change with incoming boundary-layer thickness. For both laminar and turbulent boundary layers interacting with a circular cylinder, Baker[14,23] showed that the vertical dimensions of the resulting vortex system did not change with incoming boundary-layer thickness, although the separation lines moved slightly closer to the leading edge as the boundary layer became thinner. With or without a fillet, Devenport et al.[17] also found that changes in the incoming boundary-layer thickness did not qualitatively alter the structure of the horseshoe vortex, including the surface flow visualization pattern. For flow through a turbine blade cascade, Gregory-Smith et al.[24] found no change in the position of the downstream vortex loss core with incoming boundary-layer thickness, although changes in thickness did have some effect on the intensity of the vortex loss core. This vortex loss core consists of the pressure side leg of the horseshoe vortex merged into the passage vortex.

To conclude the analysis of the surface flow visualization on the inlet guide vanes, Fig. 6 shows a reconstruction of the oil-paint pattern on the pressure surface. As with the compressor blade experiments of Dong et al.,[18] Schulz and Gallus,[19] and Joslyn and Dring,[22] the flow over the pressure surface appears very two dimensional. Similar to the suction surface, the vertical dotted lines on the pressure surface enclose a region where the oil-paint accumulated. With no adverse streamwise pressure gradient shown by Zierke et al.,[10] this oil-paint accumulation indicates natural transition. This oil-paint accumulation extended from 15 to 25% chord as shown in Fig. 7, matching fairly well with the calculated transition region ranging from 15 to 30% chord. Also shown in Fig. 6 are two dotted skin-friction lines that begin just downstream of the leading edge and move downstream in a triangular configuration. We noticed this type of pattern at various times and places on both

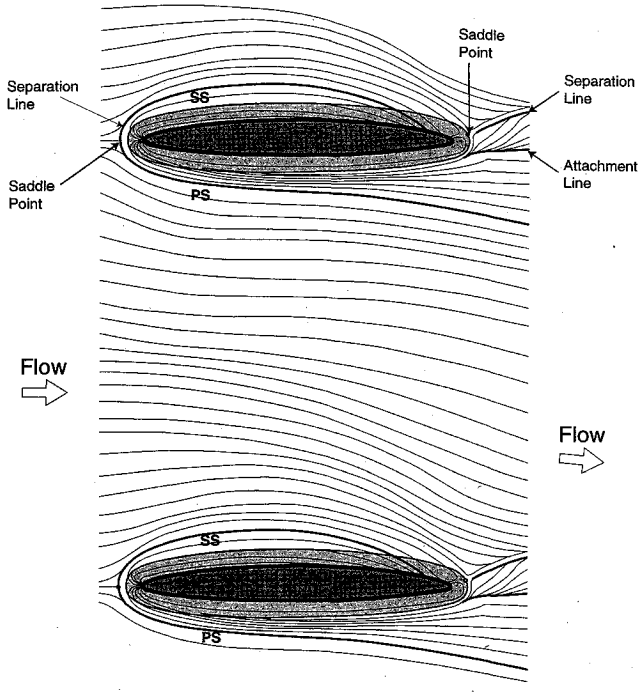

Fig. 5 Schematic of surface flow visualization on the IGV casing surface. SS = suction surface and SP = pressure surface.

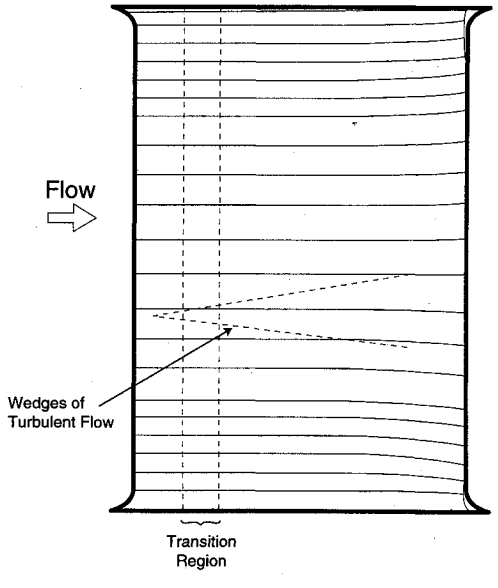

Fig. 6 Schematic of surface flow visualization on the IGV pressure surface.

the pressure and suction surfaces. Within a laminar flow region, Stanbrook[25] classified these patterns as wedges of turbulent flow from isolated excrescences. In our case, local lumps within the oil-paint or, more likely, surface irregularities, probably caused a local separation and immediate transition of the shear layer from laminar to turbulent. Notice how this wedge begins in the laminar flow region, upstream of the oil-paint accumulation that indicates natural transition.

On the pressure surface and near the trailing edge, Fig. 6 shows some radial movement of the skin-friction lines. The IGV design parameters show that the lift coefficient and circulation reach maximum values at 42% span and decrease toward both endwalls, decreasing the area within the blade section pressure distributions. Depending on the blade loading distribution, a decreasing lift corresponds to a decreasing pres-

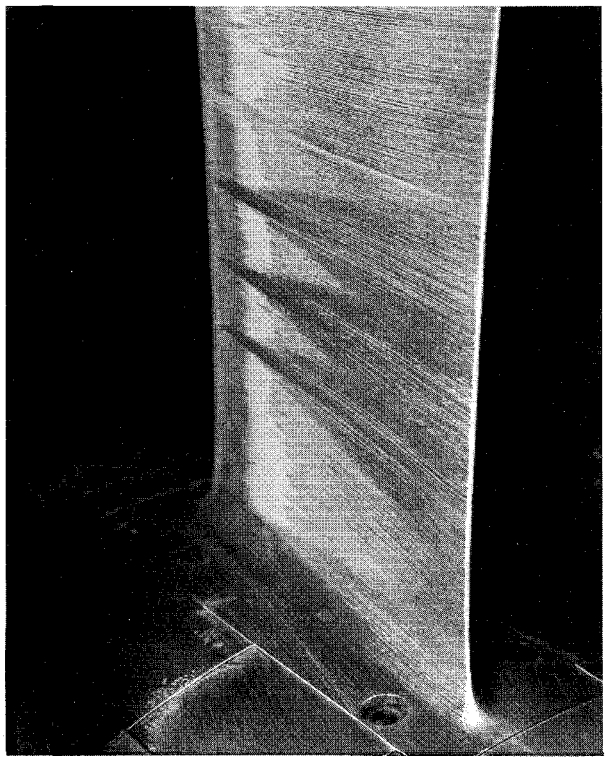

Fig. 7 Photograph of the surface flow visualization showing the IGV pressure surface (fluid flows from left to right).

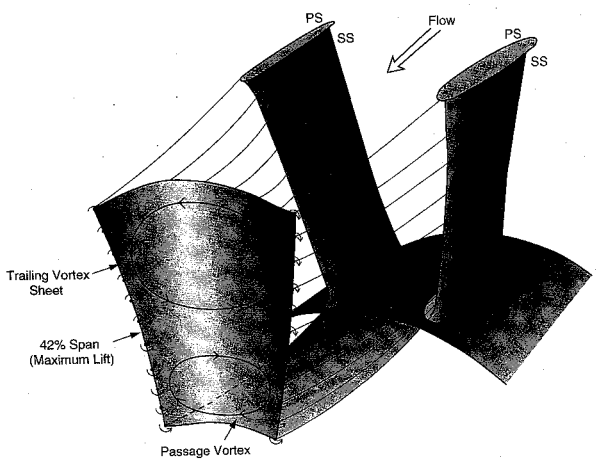

Fig. 8 Illustration of IGV secondary flow: passage vortices and trailing vortex sheets. SS = suction surface and PS = pressure surface.

sure on the pressure surface, an increasing pressure on the suction surface, or both. Therefore, the resulting radial pressure gradient can cause the flow to move radially away from the point of maximum lift on the pressure surface and/or move radially toward the point of maximum lift on the suction surface. The pressure coefficient contour plots of Zierke et al.[10] showed that the changing circulation results in a radial pressure gradient on the pressure surface, but not on the suction surface. As the boundary layers on the pressure and suction surfaces merge to form a wake, the spanwise vorticity from the pressure surface boundary layers opposes the spanwise vorticity from the suction surface boundary layers, and the resulting spanwise vorticity in the wake will eventually decay from viscous diffusion. The radial motion of the flow on the pressure surface turns a portion of the spanwise vorticity into the streamwise direction and this streamwise vorticity is shed into the wake as trailing vorticity, vorticity that will decay much slower than the spanwise vorticity in the wake. Near the hub, the resulting streamwise vorticity will be directed upstream, while near the casing, the resulting streamwise vorticity will be directed downstream. Close to the endwalls, three-dimensional effects lead to some radial flow on the suction surface that will also create streamwise vorticity.

The development of trailing vorticity from a spanwise change in circulation has been known for a long time, with a basis in three-dimensional wing theory. In turbomachinery blades, however, Smith[26] concluded that the turning of the circumferential vorticity in the incoming endwall boundary layers can also influence this trailing vortex sheet. Remember that the turning of the vorticity in an endwall boundary layer also creates the passage vortex. The blade wakes will be located between passage vortices from adjacent blade passages and these passage vortices can induce a motion within the wake opposite to the rotation in the passage vortices. Likewise, the vortex sheet created by a spanwise change in blade circulation can induce a motion within the blade passages. Actually, the vortex sheet and the passage vortices simply coexist. One is not actually the cause of the other. For a blade row such as the HIREP inlet guide vanes with a maximum circulation located near midspan, the velocities in the wakes induced by the passage vortices will likely rotate in the same direction as the trailing vortex sheet created by the spanwise gradient in circulation. Figure 8 shows how the passage vortices and trailing vortex sheets might appear downstream of the inlet guide vanes.

Results on the Rotor Blades

As with the inlet guide vanes, photographs and physical length measurements allowed us to reconstruct surface flow visualization patterns of the rotor blades on various projected surfaces. Figure 9 shows the reconstruction of the oil-paint pattern on the hub surface of the rotor blades. Again, the dark gray surface with the bold black border represents a footprint of the designed blade section at the hub, while the light gray region surrounding this blade section represents the extension of the fillet onto the hub surface. Note that the circumferential lean of the rotor blades changes how the fillet blends onto the hub surface on the pressure and suction sides of the blade. The

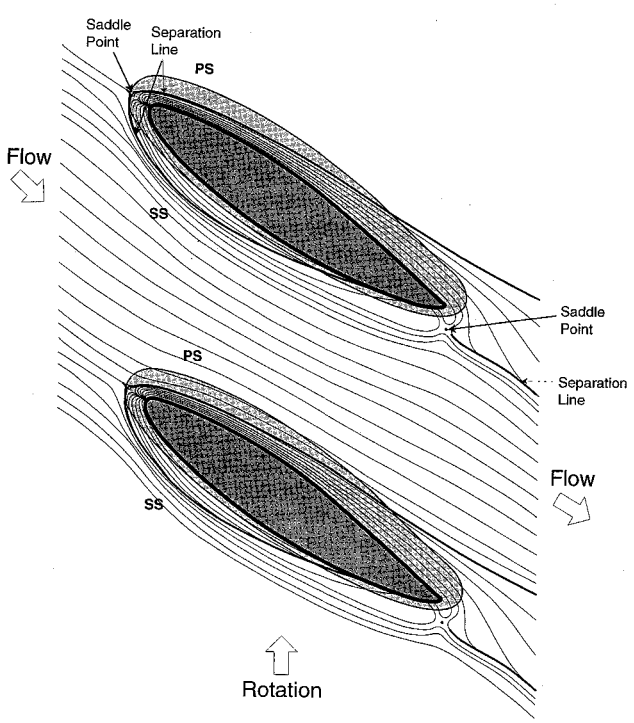

Fig. 9 Schematic of surface visualization on the rotor blade hub surface. SS = suction surface and PS = pressure surface.

relative flow vectors in Fig. 9 are the design flow vectors at the hub as determined from a streamline curvature solution.

The skin-friction lines of Fig. 9 show the same topology for the formation of the horseshoe vortex as shown on both HIREP IGV endwalls, the rotor hub surface of Dong et al.,[18] and the stator hub surface of Schulz and Gallus.[19] The saddle point was located on the outer edge of the leading-edge fillet and a line of separation passed through this saddle point, forming a C pattern. Again, we were unable to find any other critical points, critical lines, or lines of oil-paint accumulation; however, a nodal point of attachment must exist somewhere on the leading edge. The boundary layer separates along the separation line and rolls-up to form the horseshoe vortex. The pressure side leg of the horseshoe vortex convects into the midpassage region and eventually merges with the passage vortex, while the suction side leg moves up along the suction surface and eventually wraps around the passage vortex. Even for these moderately-loaded blades, a circumferential pressure gradient exists and causes the suction side leg of the separation line to move up onto the suction surface. However, comparing the exiting skin-friction lines with the design flow vector in Fig. 9 indicates that this circumferential pressure gradient produces very little overturning of the flow very close to the hub endwall. One reason for this small amount of overturning could be the blockage from what appears to be a substantial corner separation where the suction surface trailing edge meets the hub, as shown in the reconstruction of the oil-paint pattern on the suction surface in Fig. 10. Schulz and Gallus[19] found that very large corner separation regions will create a blockage that will even cause the pressure side separation line of the horseshoe vortex to be swept back towards the pressure surface.

Actually, these rotor blades were redesigned from a set of rotor blades tested by Farrell[27] to reduce the corner separation. Although the comparison of our results in Fig. 10 with those of Farrell shows some success in reducing this corner separation, the region of flow separation is still significant. This result might appear even more surprising if one notes that the diffusion factor (originally developed by Lieblein et al.[28]) at the root blade section was 0.28, well below the limiting value between 0.5–0.6 that indicates the risk of separation. However, according to Walker,[29] negative blade lean can increase the diffusion near the hub. For their compressor stator blades, Schulz and Gallus[19] also calculated diffusion factors and they showed that for small angles of attack, the corner separation region formed with a diffusion factor less than 0.4. The empirically based diffusion factor comes from two-dimensional cascade data and does not seem to correlate with three-dimensional separation. The two-dimensional boundary-layer calculations of Zierke et al.[10] also failed to indicate any separation other than very close to the trailing edge.

The topology of this three-dimensional corner separation region includes a saddle point on the hub surface of Fig. 9, just downstream of the suction side of the trailing edge. One leg of the separation line passing through this saddle point enters a spiral node of separation near 91% chord and 6% span on the suction surface, as seen in both Figs. 10 and 11. Figure 9 shows that the other leg of the separation line proceeds downstream and, beginning at the saddle point, the limiting streamlines leave the hub surface along this line to form a dividing surface of separation. The vortical core about which this dividing surface coils begins at the spiral node. Similar separation lines proceeded downstream of the trailing edge on both IGV endwall surfaces and the corresponding spiral nodes of separation seem to indicate that the dividing surfaces of separation would coil towards the suction surface (the same sense as the suction side legs of the horseshoe vortices). For the case on the rotor hub surface, the spiral node indicates that the dividing surface of separation would coil towards the pressure surface. This difference is caused by the hub rotating under this separation surface.

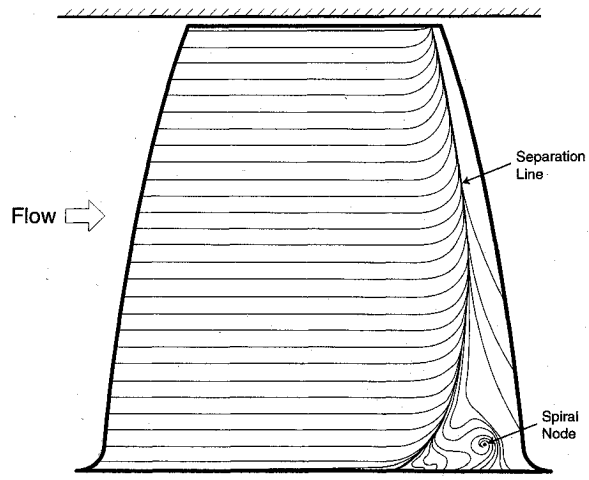

Fig. 10 Schematic of surface flow visualization on the rotor blade suction surface.

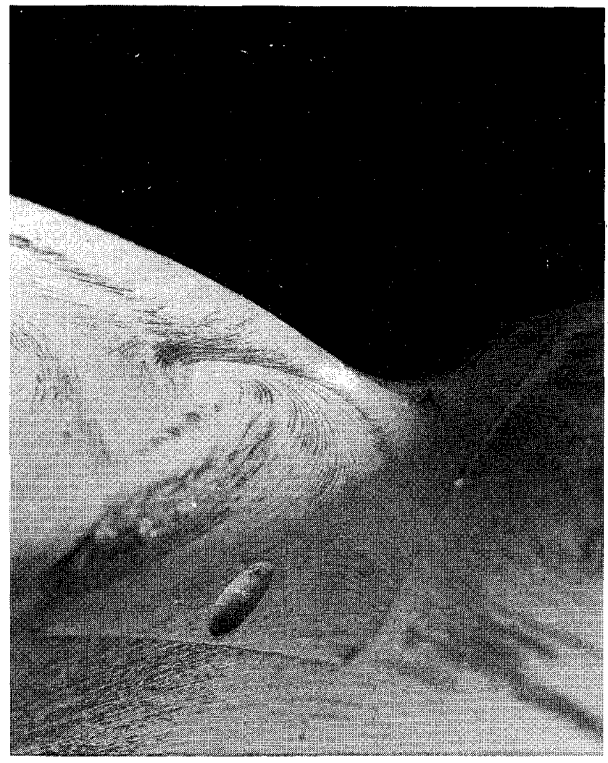

Fig. 11 Photograph of the surface flow visualization showing the rotor blade suction surface trailing-edge corner separation near the hub (fluid flow from left to right).

Figure 10 shows that a line of local separation exists on the suction surface, moving from 70% chord near the hub to 96% chord near the tip. The downstream zone of separation varies from the three-dimensional corner separation near the hub, including the spiral node of separation, to a more two-dimensional type of separation over most of the span. Just upstream of this local separation line, the skin-friction lines begin to migrate radially outward. Also, skin-friction lines emanating from the pressure surface have moved around the trailing edge within the separation zone, similar to the skin-friction lines on the stator blades of Schulz and Gallus,[19] and also migrate radially outward. Within the boundary layer, the centripetal acceleration causes the fluid to move radially outward (as explained, e.g., by Zierke et al.[10]).

Because of the radially outward flow near the trailing edge, the surface of separation that lifts off the blade at the local

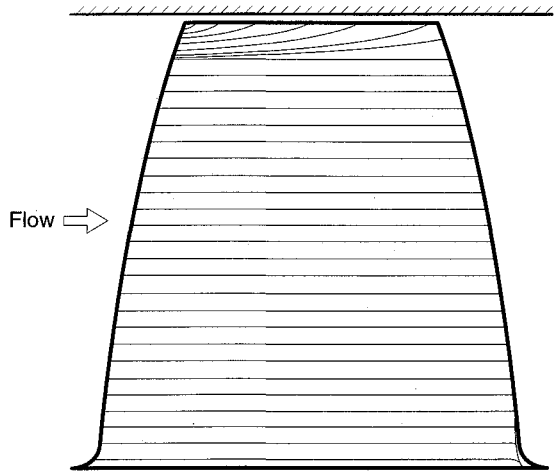

Fig. 12 Schematic of surface flow visualization on the rotor blade pressure surface.

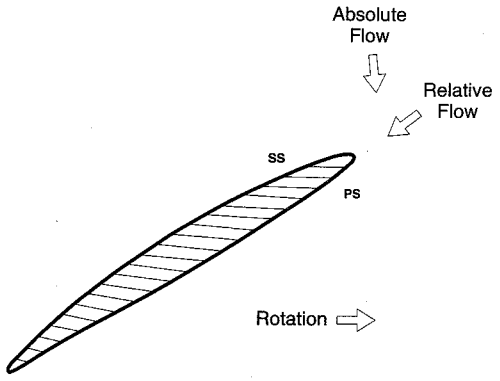

Fig. 13 Schematic of surface flow visualization on the rotor tip section. SS = suction surface and PS = pressure surface.

separation line rolls-up into a spanwise vortex. Near the casing, this vortex moves into the circumferential direction, away from the suction surface as the blade rotates in the other direction. Farrell[27] also used oil-paint surface flow visualization and found similar patterns on the suction surface of his rotor blades. In addition, he was able to visualize this vortex as it moved away from the suction surface in the circumferential direction by lowering the tunnel pressure until the vortex began to cavitate. Unfortunately, we were unable to obtain a low enough tunnel pressure for our vortex to cavitate. Evidently, the higher-loaded rotor blades used by Farrell[27] created a stronger vortex from the trailing-edge separation and the lower pressure within this vortex core led to cavitation at a higher tunnel pressure.

Figure 12 shows the reconstruction of the oil-paint pattern on the pressure surface of a rotor blade. The flow over the pressure surface appears very two dimensional. Neither the pressure nor suction surfaces on the rotor blade showed any signs of oil-paint accumulation that would indicate the presence of transition, even though boundary-layer calculations indicated that a transition region exists between 10–20% chord. One possible explanation for the failure of the oil-paint to accumulate might be the presence of wake-induced transition from the periodic passing of IGV wakes. Thus, the time-average wall shear stress becomes larger near the region where natural transition would normally occur, preventing an accumulation of the oil-paint. Also, remember that oil-paint patterns indicating natural transition depend more on oil-paint thickness and run time than do patterns indicating separation.

Near the trailing edge of the pressure surface, Fig. 12 indicates that the rotor blades exhibit more two dimensionality than the skin-friction lines for the inlet guide vanes shown in Fig. 6. Even though the rotor blade design parameters show that the lift coefficient and circulation reach maximum values at 22% span and decrease toward both endwalls, we could not clearly detect the existence of any radial motion of the skin-friction lines near the trailing edge. This does not mean that the changing spanwise circulation does not lead to a trailing vortex sheet, it simply means that we could not detect any radial motion from the photographs we had of this significantly leaned rotor blade.

One very significant pattern does show up on the pressure surface oil-paint pattern of Fig. 12: a radial outward flow exists over the top 8% of the span. A clearance exists between the rotor tip and the casing so the rotating blade avoids rubbing the casing endwall. Because of this clearance, the high-pressure fluid in the pressure surface boundary layer moves through the clearance towards the low-pressure region near the suction surface. Figure 13 shows the skin-friction lines associated with the relative leakage flow across the rotor blade tip section. Notice how these skin-friction lines on the rotor blade tip section are not parallel. Near the leading edge, the skin-friction line was tilted 1 deg from the circumferential direction, while near the trailing edge, the skin-friction line was tilted 16 deg from the circumferential direction. Also, recall that the pressure side corner of the rotor blade tip section was rounded to prevent local separation of the leakage flow; therefore, the oil-paint pattern shows no sign of separation. As the leakage flow moves through the clearance, it interacts with the through-flow across the suction surface. The interaction of these two flows causes the sheet of vorticity passing through the clearance from the pressure surface boundary layer to roll-up into a tip leakage vortex.

Summary

The analysis of the surface flow visualization on the inlet guide vanes can be summarized in Fig. 14. Note that we have performed the analysis using time-average patterns of flow separation, even though most regions of flow separation are unsteady. Figure 14 shows our interpretation of the three-dimensional skeleton structure of the secondary flow through the inlet guide vanes. The flow overturning on both endwalls moves the suction side leg of the horseshoe vortex back towards the suction surface and causes the vortex to lift off the surface. The pressure side leg of the horseshoe vortex moves into the midpassage region and eventually becomes part of

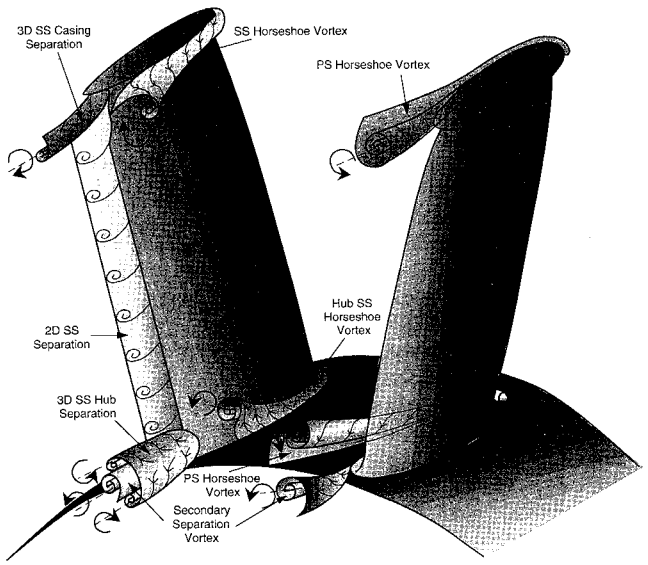

Fig. 14 Illustration of IGV secondary flow: interpretation of surface flow visualization. SS = suction surface and PS = pressure surface.

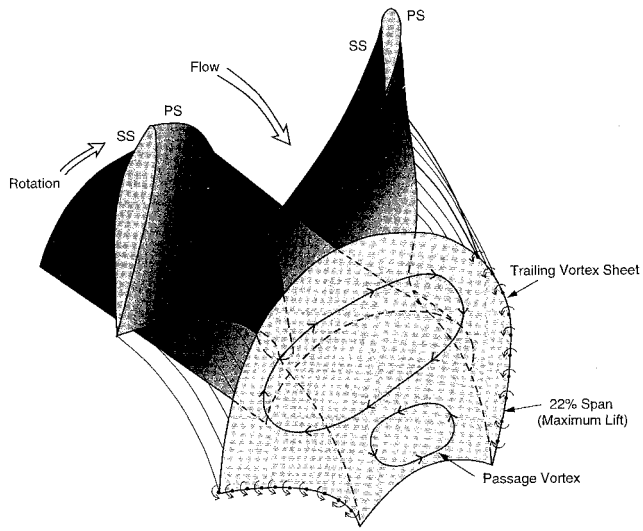

Fig. 15 Illustration of rotor blade secondary flow: passage vortices and trailing vortex sheets. SS = suction surface and PS = pressure surface.

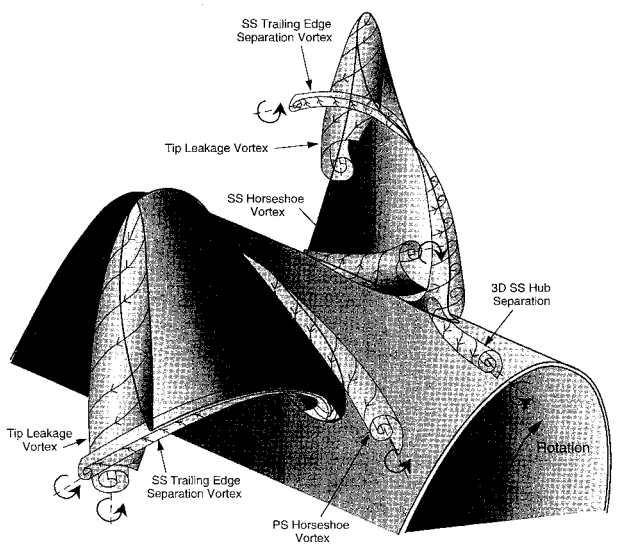

Fig. 16 Illustration of rotor blade secondary flow: interpretation of surface flow visualization.

the passage vortex illustrated in Fig. 8. Figure 14 also shows a fairly complex three-dimensional corner separation in the junction of the suction surface and the hub endwall, including a secondary separation. In the corner of the suction surface and the casing endwall, Fig. 14 shows a smaller and less complex three-dimensional separation. Finally, a two-dimensional separation occurs at the trailing edge of the suction surface.

The secondary flow downstream of the rotor blades can be summarized in Figs. 15 and 16. Figure 15 illustrates the existence of passage vortices and trailing vortex sheets, whereas Fig. 16 summarizes the analysis of the surface flow visualization on the rotor blades. Again, note that we have performed the analysis using time-average patterns of flow separation, even though most regions of flow separation are unsteady. Also, note that the secondary flows, including the skewed endwall boundary layers, developed upstream of the rotor blades can affect the incidence angle and the subsequent development of the secondary flows downstream of the rotor blades. Horlock[30] found that the effect of the secondary flow downstream of one blade row on flow turning can be the opposite of the expected effect because of the secondary flow upstream of the blade row. Within any multiple-blade-row turbomachine, one must account for the effects of secondary flow on all downstream blades.

Figure 16 shows our interpretation of the three-dimensional skeleton structure of the secondary flow through the rotor blades. The flow overturning on the hub endwall moves the suction side leg of the horseshoe vortex back towards the suction surface and causes the vortex to lift off the surface. The pressure side leg of the horseshoe vortex moves into the midpassage region and eventually becomes part of the passage vortex. Figure 16 also shows a three-dimensional corner separation in the junction where the suction surface meets the hub endwall, with a vortex filament leaving the blade surface. This three-dimensional corner separation region might be even larger if not for the presence of the periodic passing of turbulent IGV wakes over the rotor blade surfaces. Schulz et al.[31] found this to be true for their stator blade corner separation, with and without an upstream rotor blade row. Radial outward flow from centrifugal effects cause the otherwise two-dimensional separation to roll-up into a vortex, migrate up the trailing edge, and finally, move circumferentially away from the suction surface as the blade rotates. Photographs by Farrell[27] show that the trailing-edge separation vortex lies closer to the casing than the tip leakage vortex. These photographs also showed that these two vortices, rotating with the same sense, will eventually roll-up into a single vortex as they propagate downstream. The tip leakage vortex is also shown schematically in Fig. 16 and this vortex proved to be the dominant flow structure within the pump.

Conclusions

Surface flow visualization with an axial-flow pump has been used to show the topology for the formation of secondary vortical flow structures. These results led to a fairly detailed description of this complex flowfield and helped identify locations where quantitative data were measured. Comparison of these experimental time-average skin-friction lines with those obtained from numerical predictions will give an indication of whether a code can correctly predict the three-dimensional, viscous flow within an axial-flow pump. Finally, visualization of separation regions gives a designer knowledge of where to expect regions of total-pressure loss, flow deviations, cavitation, and broadband noise, knowledge that will help to direct a new design.

Acknowledgment

This investigation was supported by the Advanced Research Projects Agency.

References

[1]Squire, L. C., "The Motion of a Thin Oil Sheet Under the Boundary Layer on a Body," *Flow Visualization in Wind Tunnels Using Indicators*, compiled by R. L. Maltby, AGARDograph 70, April 1962, pp. 7–28.

[2]Tobak, M., and Peake, D. J., "Topology of Two-Dimensional and Three-Dimensional Separated Flows," AIAA Paper 79-1480, July 1979.

[3]Tobak, M., and Peake, D. J., "Topology of Three-Dimensional Separated Flows," *Annual Review of Fluid Mechanics*, Vol. 14, 1982, pp. 61–85.

[4]Arakawa, C., and Tagori, T., "Fundamental Experiments of Oil Films on a Rotating Disk," *Flow Visualization II*, edited by W. Merzkirch, *Proceedings of the 2nd International Symposium on Flow Visualization* (Bochum, Germany), 1980, pp. 127–131.

[5]Délery, J. M., "Physics of Vortical Flows," *Journal of Aircraft*, Vol. 29, No. 5, 1992, pp. 856–876.

[6]Lighthill, M. J., "Attachment and Separation in Three-Dimensional Flow," *Laminar Boundary Layers*, edited by L. Rosenhead, Sec. II 2-6, Oxford Univ. Press, Oxford, England, UK, 1963, pp. 72–82.

[7]Legendre, R., "Lignes de Courand d'un Ecoulement Permanent: Décollement et Séparation," *La Recherche Aérospatiale*, No. 6, 1977, pp. 327–335.

[8]Perry, A. E., and Fairlie, B. D., "Critical Points in Flow Patterns," *Advances in Geophysics*, Vol. 18B, Academic, New York, 1974, pp. 299–315.

[9]Hunt, J. C. R., Abell, C. J., Peterka, J. A., and Woo, H., "Kinematical Studies of the Flows Around Free or Surface-Mounted Obstacles; Applying Topology to Flow Visualization," *Journal of Fluid Mechanics*, Vol. 86, Pt. 1, 1978, pp. 179–200.

[10]Zierke, W. C., Straka, W. A., and Taylor, P. D., "The High Reynolds Number Flow Through an Axial-Flow Pump," Pennsylvania State Univ., Applied Research Lab., TR 93-12, State College, PA, Nov. 1993.

[11]Zierke, W. C., Straka, W. A., and Taylor, P. D., "An Experimental Investigation of the Flow Through an Axial-Flow Pump," *Journal of Fluids Engineering*, Vol. 117, No. 3, 1995, pp. 485–490.

[12]Farrell, K. J., McBride, M. W., and Billet, M. L., "High Reynolds Number Pump Facility for Cavitation Research," *American Society of Mechanical Engineers International Symposium on Cavitation Research Facilities and Techniques—1987*, edited by J. W. Holl and M. L. Billet, FED-Vol. 57, 1987, pp. 61–68.

[13]Gearhart, W. S., "Tip Clearance Cavitation in Shrouded Underwater Propulsors," *Journal of Aircraft*, Vol. 3, No. 2, 1966, pp. 185–192.

[14]Baker, C. J., "The Turbulent Horseshoe Vortex," *Journal of Wind Engineering and Industrial Aerodynamics*, Vol. 6, 1980, pp. 9–23.

[15]Eckerle, W. A., and Langston, L. S., "Horseshoe Vortex Formation Around a Cylinder," *Journal of Turbomachinery*, Vol. 109, April 1987, pp. 278–285.

[16]Devenport, W. J., and Simpson, R. L., "Time Dependent Structure in Wing-Body Junction Flows," *Turbulent Shear Flows VI*, Springer–Verlag, Berlin, 1988, pp. 232–248.

[17]Devenport, W. J., Agarwal, N. K., Dewitz, M. B., Simpson, R. L., and Poddar, K., "Effects of a Fillet on the Flow Past a Wing-Body Junction," *AIAA Journal*, Vol. 28, No. 12, 1990, pp. 2017–2024.

[18]Dong, Y., Gallimore, S. J., and Hodson, H. P., "Three-Dimensional Flows and Loss Reduction in Axial Compressors," *Journal of Turbomachinery*, Vol. 109, July 1987, pp. 354–361.

[19]Schulz, H. D., and Gallus, H. E., "Experimental Investigation of the Three-Dimensional Flow in an Annular Compressor Cascade," *Journal of Turbomachinery*, Vol. 110, Oct. 1988, pp. 467–478.

[20]Sieverding, C. H., "Recent Progress in the Understanding of Basic Aspects of Secondary Flows in Turbine Blade Passages," *Journal of Engineering for Gas Turbines and Power*, Vol. 107, April 1985, pp. 248–257.

[21]Sieverding, C. H., and Van den Bosch, P., "The Use of Colored Smoke to Visualize Secondary Flows in a Turbine-Blade Cascade," *Journal of Fluid Mechanics*, Vol. 134, Sept. 1983, pp. 85–89.

[22]Joslyn, H. D., and Dring, R. P., "Axial Compressor Stator Aerodynamics," *Journal of Engineering for Gas Turbines and Power*, Vol. 107, No. 2, 1985, pp. 485–493.

[23]Baker, C. J., "The Laminar Horseshoe Vortex," *Journal of Fluid Mechanics*, Vol. 95, Pt. 2, Nov. 1979, pp. 347–368.

[24]Gregory-Smith, D. G., Graves, C. P., and Walsh, J. A., "Growth of Secondary Losses and Vorticity in an Axial Turbine Cascade," *Journal of Turbomachinery*, Vol. 110, Jan. 1988, pp. 1–8.

[25]Stanbrook, A., "The Surface Oil Flow Technique for Use in High Speed Wind Tunnels," *Flow Visualization in Wind Tunnels Using Indicators*, compiled by R. L. Maltby, AGARDograph 70, April 1962, pp. 39–49.

[26]Smith, L. H., Jr., "Secondary Flow in Axial-Flow Turbomachinery," *Transactions of the American Society of Mechanical Engineers*, Vol. 77, Oct. 1955, pp. 1065–1076.

[27]Farrell, K. J., "An Investigation of End-Wall Vortex Cavitation in a High Reynolds Number Axial-Flow Pump," M.S. Thesis, Dept. of Mechanical Engineering, Pennsylvania State Univ., State College, PA, May 1989.

[28]Lieblein, S., Schwenk, F. C., and Broderick, R. L., "Diffusion Factor for Estimating Losses and Limiting Blade Loadings in Axial-Flow-Compressor Blade Elements," NACA RM E53 D01, June 1953.

[29]Walker, P. J., "Blade Lean in Axial Turbines: Model Turbine Measurements and Simulation by a Novel Numerical Method," Ph.D. Dissertation, Dept. of Engineering, Univ. of Cambridge, Cambridge, England, UK, Dec. 1987.

[30]Horlock, J. H., "Annulus Wall Boundary Layers in Axial Compressor Stages," *Journal of Basic Engineering*, Vol. 85, No. 1, 1963, pp. 55–65.

[31]Schulz, H. D., Gallus, H. E., and Lakshminarayana, B., "Three-Dimensional Separated Flow Field in the Endwall Region of an Annular Compressor Cascade in the Presence of Rotor-Stator Interaction: Part I—Quasi-Steady Flow Field and Comparison with Steady-State Data," *Journal of Turbomachinery*, Vol. 112, No. 4, 1990, pp. 669–678.